Front. Earth Sci. 2025, 19(4): 566−584
https://doi.org/10.1007/s11707-024-1122-1

RESEARCH ARTICLE

Lithofacies assemblages of shale and dense shell limestone: implications for shale oil exploration

Yixin ZHOU[1,2,3], Zhenglu XIAO (✉)[1,2,3], Yong LI[1,2,3], Jungang LU (✉)[1,2,3], Qijun JIANG[3], Xiang ZHOU[3], Ziyi CAI[3], Xiyuan WANG[3]

1 State Key Laboratory of Oil and Gas Reservoir Geology and Exploitation, Southwest Petroleum University, Chengdu 610500, China
2 Natural Gas Geology Key Laboratory of Sichuan Province, Southwest Petroleum University, Chengdu 610500, China
3 School of Geoscience and Technology, Southwest Petroleum University, Chengdu 610500, China

Abstract Assemblages of limestone and shale have been proven favorable shale oil-producing layers in North American and Chinese basins. However, the Jurassic Da'anzhai Formation in the Sichuan Basin did not meet these expectations. The relationship between the lithofacies assemblages and shale oil enrichment was investigated based on FE-SEM, XRD, N_2 adsorption, HPMI, NMR, and rock pyrolysis experiments. The results showed that ten main lithofacies developed in the Da'anzhai Formation. The undeveloped dissolution pores in the shell limestone led to clay intergranular pores and microfractures constituted the main oil reservoir space. With increased shale content, the physical properties and oil content gradually improved. These special geological conditions indicate that the breakthrough of shale oil in the Da'anzhai Formation depends only on the developed fracture system. A favorable exploration target was the layered lithofacies with developed veined calcite and bedding fractures. The results obtained in this study are significant for shale oil exploration of the same type of lithological assemblage worldwide.

Keywords shale oil, lithofacies, pore structure, Da'anzhai Formation, Sichuan Basin

1 Introduction

With the significant success of shale oil development in North America, shale oil has become an important part of the global energy industry chain, and an increasing number of countries are becoming increasingly important. According to the Energy Information Administration (EIA), Advanced Resources International, Inc. (ARI), China National Petroleum Corporation (CNPC), and China Petroleum & Chemical Corporation (SNP), the total exploitable shale oil resources worldwide are approximately 47.1 billion tons, distributed across 104 basins in 46 countries (EIA, 2015; ARI, 2015). China's developable shale oil resources exceed 3 billion tons, ranking third worldwide (Zou et al., 2013; ARI, 2015). This huge resource potential has driven the large-scale commercial development of shale oil in China.

Exploration experience has shown that underground sandstone or carbonate rocks have better reservoir and fracturing properties than shale. Therefore, sandstone and limestone interlayers in thick shale formations are favorable exploration targets for shale oil. Based on this principle, China has successively conducted shale oil explorations in major basins and achieved remarkable results. China has achieved small-scale exploitation of shale oil in the Junggar, Ordos, Songliao, and Bohai Bay Basins (Zhao et al., 2020; Li et al., 2022a; Hu et al., 2022). According to successful exploration and development experience, the shell limestone interlayers in the Jurassic Da'anzhai Formation are also considered favorable conditions for shale oil development.

To investigate the shale oil development potential of the Da'anzhai Formation in the Sichuan Basin, more than ten wells have been deployed in the CNPC and SNP since 2019. So far, only the LA1 (gas 2000 m^3/day; oil 1.76 tons/day) and LX1 (gas 3.36 × 10^4 m^3/day; oil 22.4 m^3/day) wells have achieved limited success. Both of these wells have geological conditions of high maturity (R_o > 1.5%), high formation pressure coefficient (> 1.3), and high organic matter abundance (TOC > 1.5%) (He et al., 2022). This sharply contrasts with the major shale oil-producing layers worldwide (Jarvie, 2012; Liu et al., 2021b). Therefore, shale oil development in the Da'anzhai Formation has reached a bottleneck.

To investigate the particularity of limestone and shale

Received November 29, 2023; accepted March 6, 2024

E-mails: 18428372745@163.com (Zhenglu XIAO)
lujungang21@sohu.com (Jungang LU)

assemblages, this study used advanced technical means to evaluate different lithofacies' reservoir properties, oil-bearing, and oil-movable conditions. The reasons for unsuccessful exploration were analyzed, and favorable exploration targets were identified. This study provides a theoretical basis and technical support for shale oil exploration in the Da'anzhai Formation of the Sichuan Basin. This is also important for shale oil exploration in limestone and shale assemblages worldwide.

2 Geological background

The Sichuan Basin is located in southwest China, between north latitude 28°–32°40′ N and east longitudes 102°30′–110° E, with a total area of approximately 18 × 10^4 km^2 (Li et al., 2020; Xiao et al., 2021; Wang et al., 2024). The Sichuan Basin is a large negative tectonic basin formed by the compression and collision of the Indian and Eurasian plates, which also caused the overall uplift of the Yangtze platform (Fig. 1(a)) (Liu et al., 2016). The Sichuan Basin is located to the north of the Yangtze Platform (Fig. 1(b)). Its western edge is the Longmen Mountain fault zone, its northern edge is Micang Mountain, its north-eastern edge is the Daba Mountain and Qiyue Mountain fold zones, its south-eastern edge is the Daluoshan fold zone, and its south-

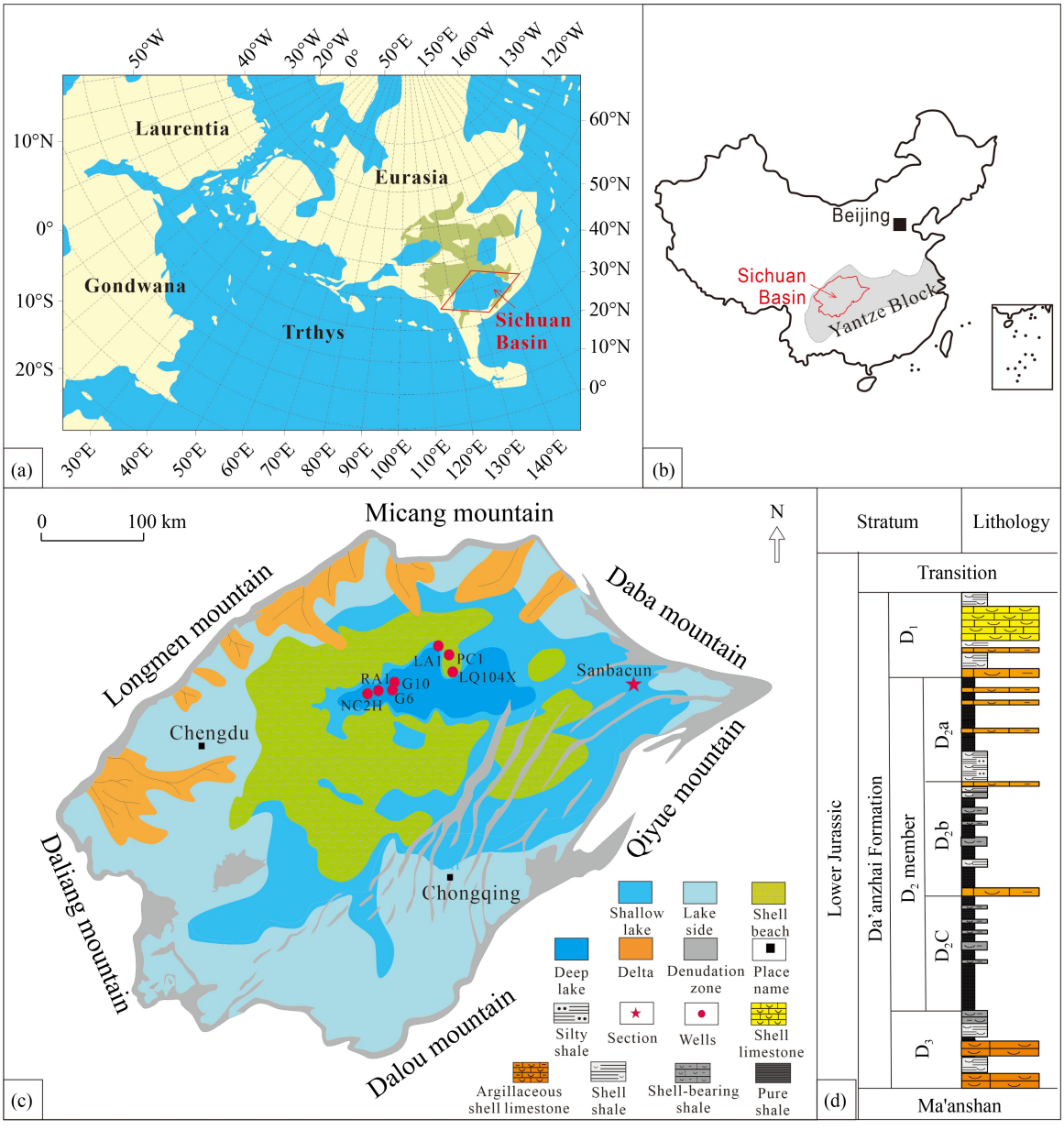

Fig. 1 Location and geological framework of Sichuan Basin. (a) Early Jurassic Global Palaeogeographical World Map; (b) development area of the Upper Yangtze Platform in China; (c) Sichuan Basin structure and sedimentary facies of Da'anzhai Formation; (d) stratigraphic characteristics of Jurassic Da'anzhai Formation.

western edge is the Emei-Daliang Mountain fault zone (Fig. 1(c)).

The Da'anzhai Formation records the largest lake leaching in the Sichuan Basin and develops its primary source rocks (Su et al., 2018; Zhang et al., 2022a). From the plane view (Fig. 1(c)), when the Da'anzhai Formation was deposited, the Nanbu-Yingshan area was the sedimentary center, and half-deep lake mud developed. Large-scale shell beaches have developed in shallow lakes (Lei et al., 2023; Xu et al., 2023). The thickness of the Da'anzhai Formation is 60–100 m. According to its sedimentary evolution, it can be divided into three members from bottom to top: D_3, D_2, and D_1 (Fig. 1(d)). The D_2 member is further divided into three sub-members: D_2a, D_2b, and D_2c.

The thickness of the D_3 member is 5–15 m, and the lithology is mainly composed of thick blocks of brownish-gray shell limestone with thin layers of black shale. The D_2 member has a thickness of 35–60 m, mainly developing thick black shale with differences in lithology among each sub-member (Zhang et al., 2022a). The D2a sub-member typically develops an interlayer of black shale and shell limestone. The lithology of the D_2b sub-member is mainly thick black shale with thin layers of shell limestone. Thick, massive black shales develop in the D_2c sub-member. The thickness of the D_1 sub-member is 20–30 m, mainly developing thick-shelled limestone (Chen et al., 2020).

3 Samples and methods

3.1 Samples

Eight rock samples from wells G6 and RA1 were observed using a polarization microscope and field emission scanning electron microscopy (FE-SEM). X-ray diffraction (XRD) tests were performed on 74 samples from wells PC1, G10, NC2H, and LA1. Eleven rock samples from PC1 and G10 were tested for low-temperature N_2 adsorption (Table 1). High-pressure mercury injection (HPMI) testing was performed on five samples collected from wells RA1, PC1, and G10 (Table 2). The nuclear magnetic resonance (NMR) experiments were conducted on 15 samples from well LA1 (Table 3). Rock pyrolysis analysis of samples from wells PC1, G10, RA1, LA1, and LQ104X was conducted. Rock pyrolysis data were obtained from the Exploration and Development Research Institute of the PetroChina Southwest Oil and Gas Field Company.

3.2 Experimental methods

3.2.1 FE-SEM

Scanning electron microscopy (SEM) was performed using an FEI Quanta 650 FEG field-emission scanning electron microscope. The samples were prepared into rectangular blocks with a length of 8 mm, a width of 8 mm, and a height of 3 mm and were then ground with ultra-thin emery paper with particle sizes of 30 μm, 15 μm, 9 μm, 6 μm, 3 μm, 1 μm, and 0.1 μm until the surface was flat. Polishing was then performed under vacuum using a Hitachi IM 4000 argon-ion polisher. The polished thick shale samples were imaged with secondary electrons using a Hitachi dual-beam scanning electron microscope to obtain high-resolution pore structure images.

3.2.2 XRD

X-ray diffraction analysis is currently a simple and

Table 1 N_2 adsorption experimental data of Da'anzhai Formation shale in the Sichuan Basin

Well	Sample number	Depth/m	Hysteresis loop type	BET-SSA/ ($m^2 \cdot g^{-1}$)	DFT		
					SSA/($m^2 \cdot g^{-1}$)	TPV/($cm^3 \cdot g^{-1}$)	Dp/nm
PC1	1	3210.19	H2	9.708	3.975	0.013	3.136
	2	3217.40	H3-H4	3.507	2.079	0.007	2.971
	3	3209.55	H2-H3	5.679	3.188	0.012	3.135
	4	3239.15	H2-H3	5.831	4.047	0.016	2.969
	5	3245.07	H2	10.632	3.544	0.012	3.131
	6	3247.79	H2	11.266	4.117	0.014	3.132
G10	7	2680.58	H3	2.133	1.918	0.012	2.973
	8	2681.00	H3	2.723	2.319	0.014	2.978
	9	2681.90	H3	2.489	2.124	0.012	3.327
	10	2682.40	H3-H4	1.508	1.365	0.008	3.137
	11	2685.90	H2-H3	5.036	2.69	0.01	3.131

Notes: SSA-specific surface area, TPV-total pore volume, Dp-pore diameter.

Table 2 High-pressure mercury injection test data of Da'anzhai Formation rock samples in the Sichuan Basin

Well	Sample number	Depth/m	Lithofacies type	Threshold pressure/ Psia	Porosity/ %	Average Dp/ nm	TPV/ ($mL \cdot g^{-1}$)	SSA/ ($m^2 \cdot g^{-1}$)
RA1	1	2471.00	F	5.68	1.951	205.430	0.008	0.145
	2	2473.77	C	3.43	3.847	16.500	0.015	3.651
	3	2487.60	I	0.67	2.532	36.560	0.010	1.077
G10	4	2686.70	J	12.97	7.680	15.980	0.033	8.254
PC1	5	3180.01	A	3.38	1.401	651.970	0.005	0.033

Notes: SSA-specific surface area, TPV-total pore volume, Dp-pore diameter.

Table 3 NMR statistics of rock samples from Da'anzhai Formation of Well LA1 in the Sichuan Basin

Lithofacies type	Depth/m	Average aperture/nm	Peak area of pores with different sizes		
			Micropore (P_1 Peak)	Mesopore (P_2 Peak)	Macropore (P_3 Peak)
A	3470.23	154.16	12.57	88.50	315.93
	3476.02	228.41	13.02	43.41	350.91
	3485.72	191.26	12.05	24.94	/
C	3493.36	47.13	28.39	48.99	12.72
	3503.25	5.94	79.46	79.46	435.07
F	3496.06	425.82	112.07	41.75	/
	3478.75	9.88	49.16	93.55	844.80
	3493.31	99.54	29.66	71.74	562.54
	3511.96	160.92	87.32	282.63	951.91
I	3534.69	136.29	104.72	239.23	/
	3540.16	114.26	106.35	202.73	258.86
	3546.17	209.73	61.03	185.58	685.72
J	3504.67	514.64	130.53	216.72	/
	3506.69	379.60	110.72	285.42	1393.20
	3536.19	161.80	100.53	227.56	174.78

efficient experimental method for identifying, analyzing, and quantifying the characteristics of shale mineral compositions. A small shale sample was first ground to 200 mesh and dried at 110°C. A PANalytical X' Pert PRO X-ray diffractometer was used in the experiments. The instrument was equipped with a Co target and operated at 31 kV and 0.4 mA. Diffraction angles (2θ) were measured over a range of 3°–55° with a scanning interval of 0.02° (2θ). Semiquantitative analysis was performed using the X-Powder software.

3.2.3 N_2 adsorption and desorption

First, approximately 3 g of the shale sample was weighed and crushed to pass through a 60–120 mesh sieve. Then, the samples were degassed and dried at 110°C and a vacuum of less than 10 mmHg for more than 10 h. The experiment was performed using a Quantachrome NOVA4200e specific surface-area porosimeter. The relative pressure was set to 0.005–0.995. Using high-purity N_2 as the adsorbate, an adsorption curve under liquid-nitrogen temperature conditions was obtained.

3.2.4 HPMI

The sample was cut into small cubes (1.0 cm^3) with a cutting machine. The samples were washed with organic solvent and dried for 2 h at 110°C for dehydration. After the pretreatment, the samples were loaded into a dilatometer with a volume of 1 cm^3, taking care to prevent secondary contamination. The dilatometer containing the sample was transferred to a pore gauge and vacuumed under low pressure for degassing. Finally, the pore structure data of the samples were obtained using a Quantachrome Pore Master GT 60 automatic mercury intrusion instrument (Konta, USA).

3.2.5 NMR

Core plug samples were used for the NMR experiments. The samples were placed in a vacuum saturation chamber and evacuated for 1 h to remove air and adsorbed

impurities. The samples were then saturated with crude oil at a fluid pressure of 30 MPa for 24 h for NMR testing. The nuclear magnetic resonance experimental instrument was a MesoMR23/12-060H-I nuclear magnetic NMR instrument produced by the Niumag Company. The magnetic field strength was 0.3 ± 0.03 T. The primary frequency (SF) was 12 MHz. NMR T_2 analysis adopted CPMG echo sequence, and the experimental parameters were set as echo interval time (TE) 0.1 ms, echo number (NECH) 16000, waiting time (TW) 6 000 ms, scan number (NS) 32.

3.2.6 Rock pyrolysis

Approximately 10 mg of powdered rock samples was prepared. Experiments were performed using a Vinci Rock-Eval 6 instrument. The total organic carbon (TOC, wt.%), free hydrocarbon (S_1, mg/g), pyrolytic hydrocarbon (S_2, mg/g), and maximum pyrolysis temperature (T_{max}, °C) were obtained. The oil content index (S_1/TOC) was calculated to characterize the oil content of the shale.

4 Results

4.1 Mineral composition

The XRD results of the 74 samples showed that the main mineral components were quartz, calcite, and clay. The proportions of plagioclase, dolomite, and pyrite were relatively low. In comparison (Fig. 2), the clay mineral content was the highest, averaging 48% (19%–71%). The quartz content took second place, averaging 30% (10%–49%). The calcite content was relatively low, averaging 13% (0%–64%). The average plagioclase, dolomite, and pyrite contents were less than 5%.

4.2 Organic geochemical characteristics

The rock pyrolysis test results showed that the TOC content of the shale was between 0.09% and 5.58%, with an average value of 1.38%. The S_1 value was between 0.01 mg/g and 9.47 mg/g, with an average value of 1.05 mg/g. The value of $S_1 + S_2$ was between 0.04 mg/g and 26.97 mg/g, with an average of 3.64 mg/g. As seen from the cross-plot of TOC and $S_1 + S_2$ (Fig. 3), the abundance of organic matter in the Da'anzhai Formation shale was mainly at a medium-good level, and some samples (accounting for 16.0%) reached an excellent level. The S_2-TOC chart was selected to distinguish the organic matter type of the shale (Fig. 4) (Langford and Blanc-Valleron, 1990; Elika et al., 2006), which showed that the organic matter type of the shale was mainly types II and III. The average value of T_{max} was 443°C (320°C–485°C), indicating the samples have reached maturity to high maturity.

4.3 Pore structure characteristics

4.3.1 N_2 adsorption

The results of the low-temperature N_2 adsorption experiments showed that the samples had different curve shapes (Fig. 5). According to the classification of IUPAC (the International Union for Pure and Applied Chemistry), four curve shapes were identified: H_2 (Fig. 5(a)), mixed H_2 and H_3 (Fig. 5(b)), H_3 (Fig. 5(c)), and mixed H_3 and H_4 (Fig. 5(d)).

The BET-specific surface area (SSA), total pore volume (TPV), and pore diameter (Dp) of crushed samples can be obtained by analyzing N_2 adsorption data (Clarkson et al., 2011; Han et al., 2016). From the statistical results (Table 1), the SSA, TPV, and Dp of the H_2 type were relatively high, with average values of

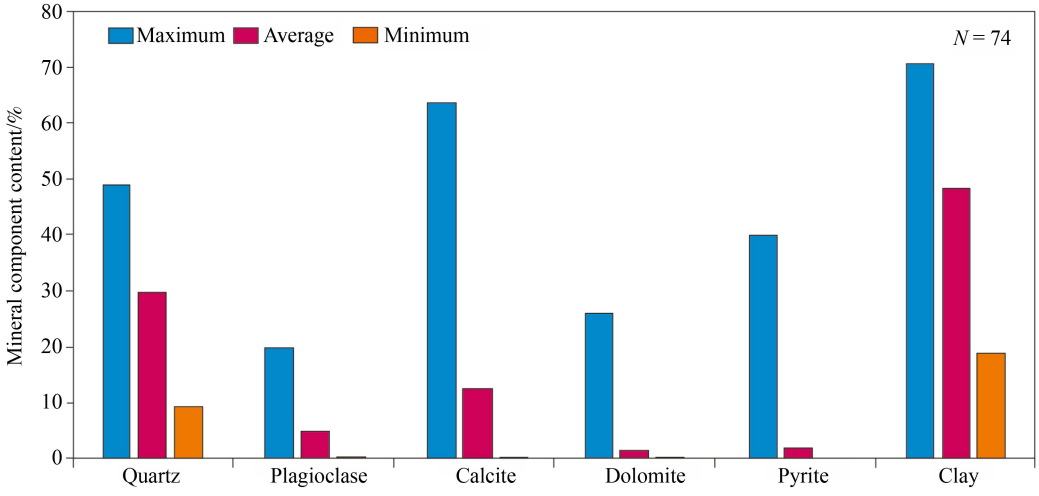

Fig. 2 Statistical histogram of the mineral content of Da'anzhai Formation shale in the Sichuan Basin.

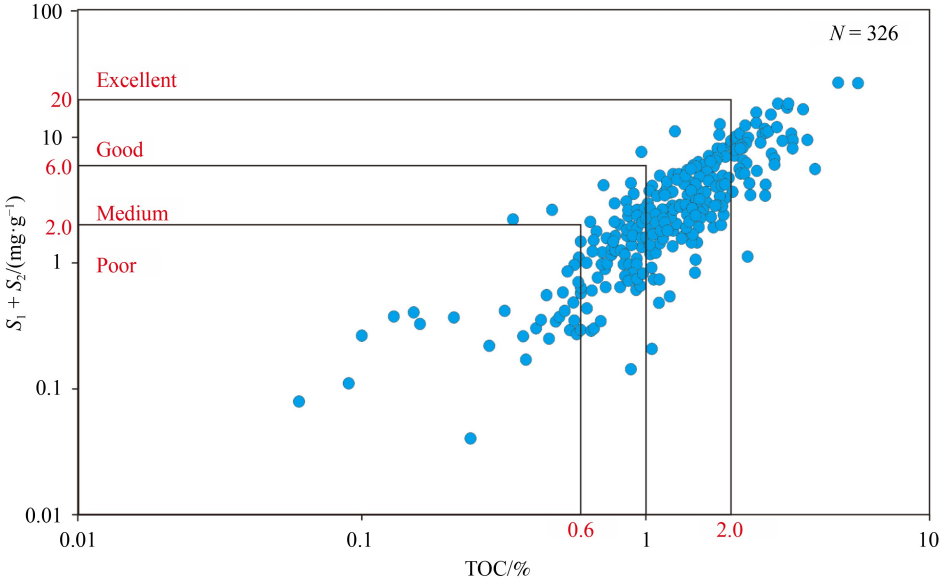

Fig. 3 Identification chart of organic matter abundance of Da'anzhai Formation shale in the Sichuan Basin.

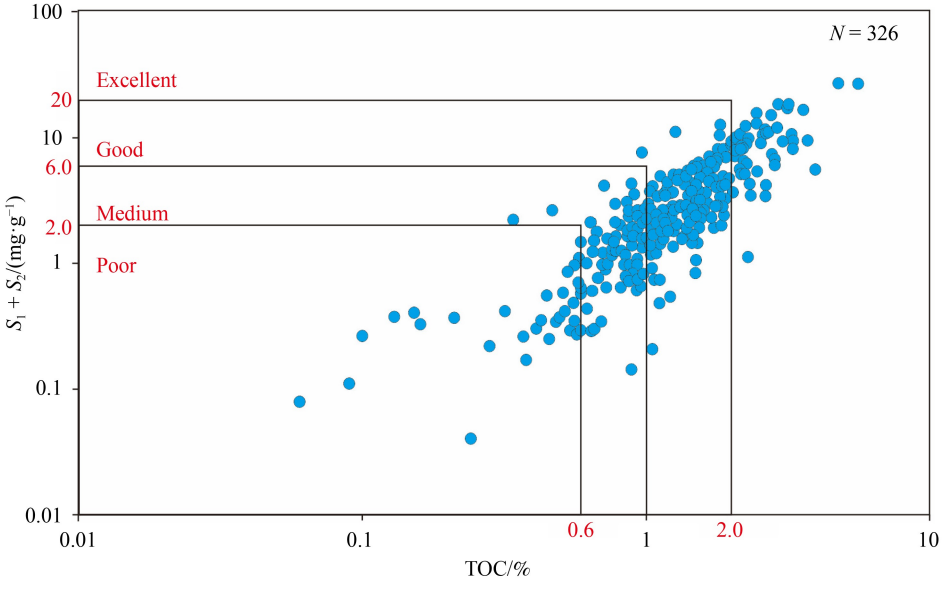

Fig. 4 Identification chart of organic matter type of Da'anzhai Formation shale in the Sichuan Basin.

10.535 m^2/g, 0.0130 cm^3/g, and 3.133 nm, respectively. The SSA, TPV, and Dp of the mixed types of H_2 and H_3 ranked second, with average values of 5.515 m^2/g, 0.0127 cm^3/g, and 3.078 nm, respectively. The SSA, TPV, and Dp values of the H_3 type were small, with average values of 2.448 m^2/g, 0.0127 cm^3/g, and 3.093 nm, respectively. The SSA, TPV, and Dp of the mixed type of H_3 and H_4 were the smallest, with average values of only 2.507 m^2/g, 0.0075 cm^3/g, and 3.054 nm, respectively.

4.3.2 HPMI

The results of the HPMI test (Table 2) showed that the Da'anzhai Formation reservoir was generally tight. The porosity was between 1.40%–7.68%, and the threshold pressure was 0.67–12.97 MPa. The pore structures of different samples varied significantly. The TPV was 0.005–0.033 mL/g, and the average pore diameter was 15.98–651.97 nm. Interestingly, the porosity, TPV, and SSA were positively correlated with each other but negatively correlated with the pore diameter. This phenomenon indicates that the Da'anzhai Formation has abnormal characteristics of independent macropores and intensive micropores. As shown in the cumulative mercury intake and pore diameter distribution curves (Fig. 6), the pore diameters of the study samples were mainly below 100 nm.

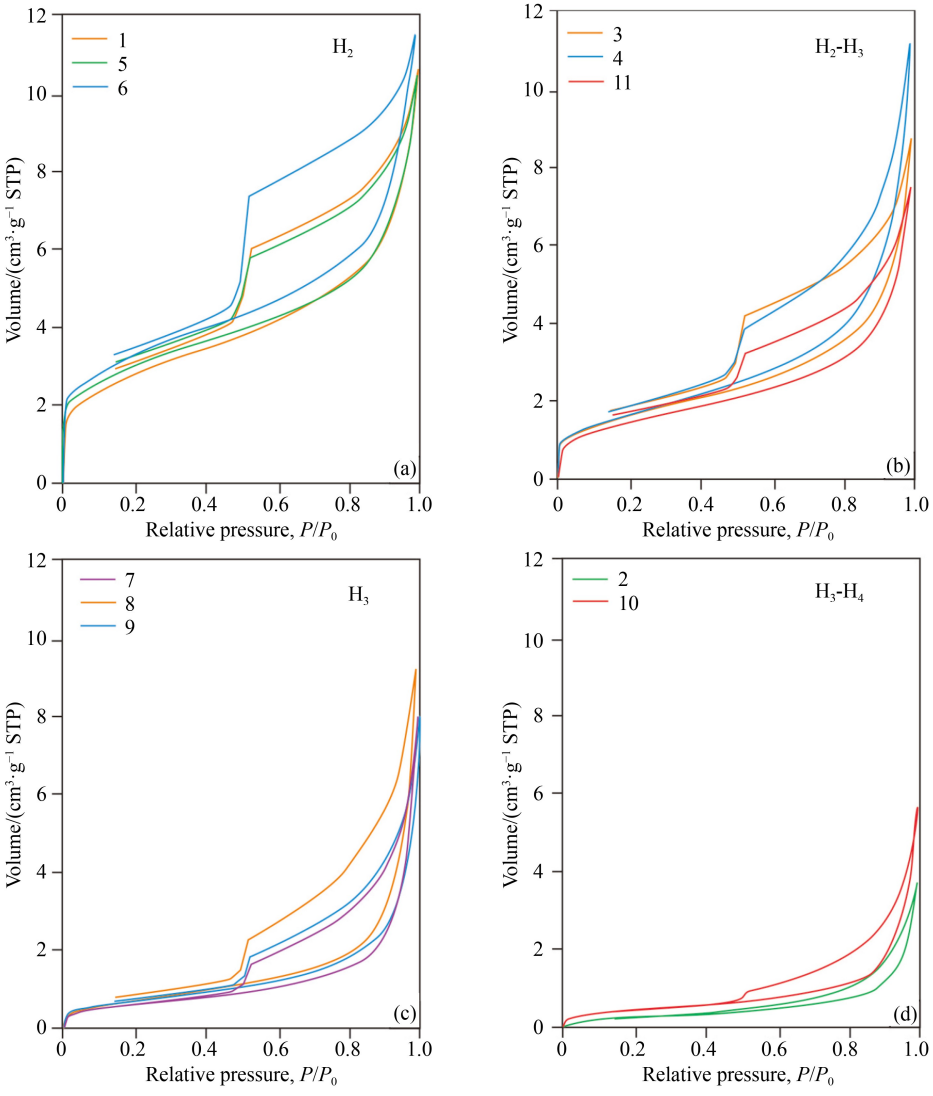

Fig. 5 N_2 adsorption and desorption curve of Da'anzhai Formation shale in the Sichuan Basin.

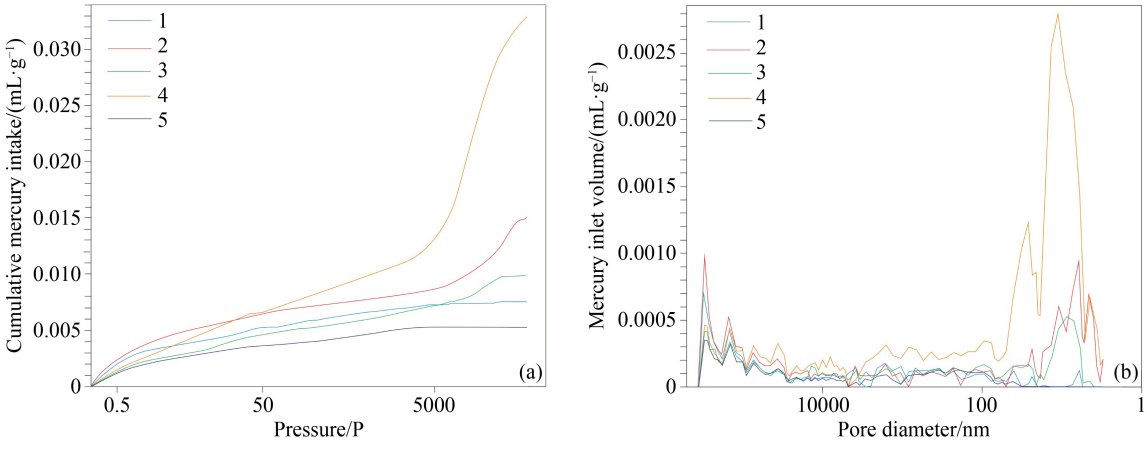

Fig. 6 (a) High-pressure mercury injection curve and (b) pore diameter distribution of different samples from the Da'anzhai Formation in the Sichuan Basin.

4.3.3 NMR

The T_2 distribution of the rock samples saturated with oil exhibited a three-peak shape (P_1, P_2, and P_3) (Fig. 7), indicating that the pore structure was relatively complex. In general, the P_1 peak fallss within the range of T_2 <

10 ms, the P_2 peak within 10 ms < T_2 < 100 ms, and the P_3 peak within 100 ms < T_2 < 1000 ms. Zhang et al. (2022b) proposed that the three peaks in the NMR spectrogram represent micropores, mesopores, and macropores, respectively. Among the three peaks of the Da'anzhai Formation samples, the P_1 peak showed the strongest signal. In contrast, the P_2 and P_3 peaks had weak signals, indicating that the proportion of micropores in all samples is relatively large.

5 Discussion

5.1 Lithofacies types and assemblages

Research on shale lithofacies is scarce. Researchers have used various lithofacies classification schemes for different purposes. For example, Loucks and Ruppel (2007) divided lithofacies by combining rock mineral components with total organic carbon (TOC). Liu et al. (2018) divided lithofacies by comprehensively considering rock structure, organic matter abundance, and mineral composition. Yue et al. (2021) classified lithofacies based on the mineral composition of rocks. Feng et al. (2021) classified lithofacies based on sedimentological and ichnological characteristics. Mohammed et al. (2022) divided lithofacies according to differences in their biological types. Given the critical role of rock structure in shale oil occurrence and flow, this study combined rock structure and lithology to divide the lithofacies.

5.1.1 Rock structures

Based on core observations and microscopic identification, the rock structure of the Da'anzhai

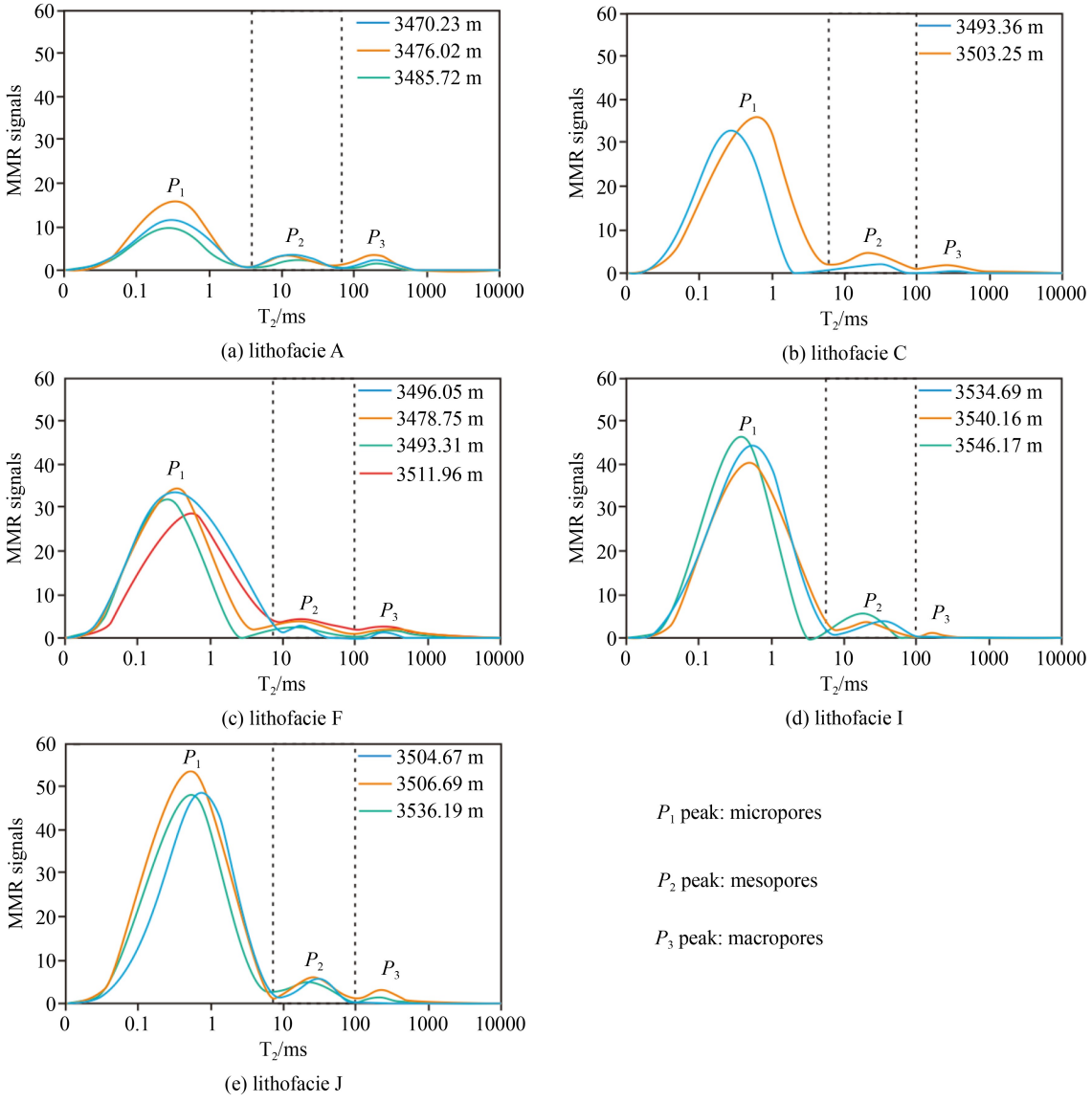

Fig. 7 NMR T_2 spectra of saturated water rock samples of Da'anzhai Formation in the Sichuan Basin.

Formation is generally divided into four types: massive, layered, laminated, and foliated. Shell limestone (Figs. 8(a) and 8(h)), argillaceous shell limestone (Figs. 8(b) and 8(i)), and shell-bearing shale (Figs. 8(c) and 8(j)) exhibit massive structures. The hybrid sedimentary rocks of shale, shell limestone, and siltstone were generally layered (Figs. 8(d), 8(e), and 8(k)) or laminated (Figs. 8(f) and 8(l)), and the organic-rich shale was foliated (Figs. 8(g) and 8(m)). The calcareous bands in the hybrid sedimentary rocks were mainly composed of veined calcite with a superimposed structure (Figs. 8(n) and 8(o)).

5.1.2 Lithology and Lithofacies

The lithology was classified using a ternary diagram of mineral components (Hickey and Henk, 2007; Lazar et al., 2015; Liu et al., 2020). The composition plots of the 78 samples revealed that eight lithologies are mainly developed in the Da'anzhai Formation (Fig. 9). Shale can be classified into silty and silty-bearing clayey shales. Small amounts of shell shale, shell-bearing clayey shale, and clayey shale are also observed. The carbonate rocks can be subdivided into shell limestones and argillaceous shell limestones. A certain proportion of argillaceous siltstones also present. According to the rock structure and lithology, the Da'anzhai Formation can be divided into ten lithofacies (Fig. 10): A-massive shell limestone; B-massive argillaceous shell limestone; C-massive shell-bearing clayey shale; D-massive clayey shale; E-layered argillaceous shell limestone; F-layered shell shale; G-layered silty shale; H-layered argillaceous siltstone; I-laminated shell-bearing clayey shale; J-foliated silty-bearing clayey shale.

The lithofacies reflect a relatively fine (decimeter scale) sedimentary environment. However, it is difficult to guide the exploration of shale oil based on lithofacies because of the variable sedimentary environment and frequent overlapping of lithofacies in a set of strata. Therefore, it is necessary to divide the larger scale (meter scale) lithological assemblages according to the overall evolutionary trend of the sedimentary environment (Bai et al., 2020; Mohammed et al., 2022; Nabawy et al., 2022).

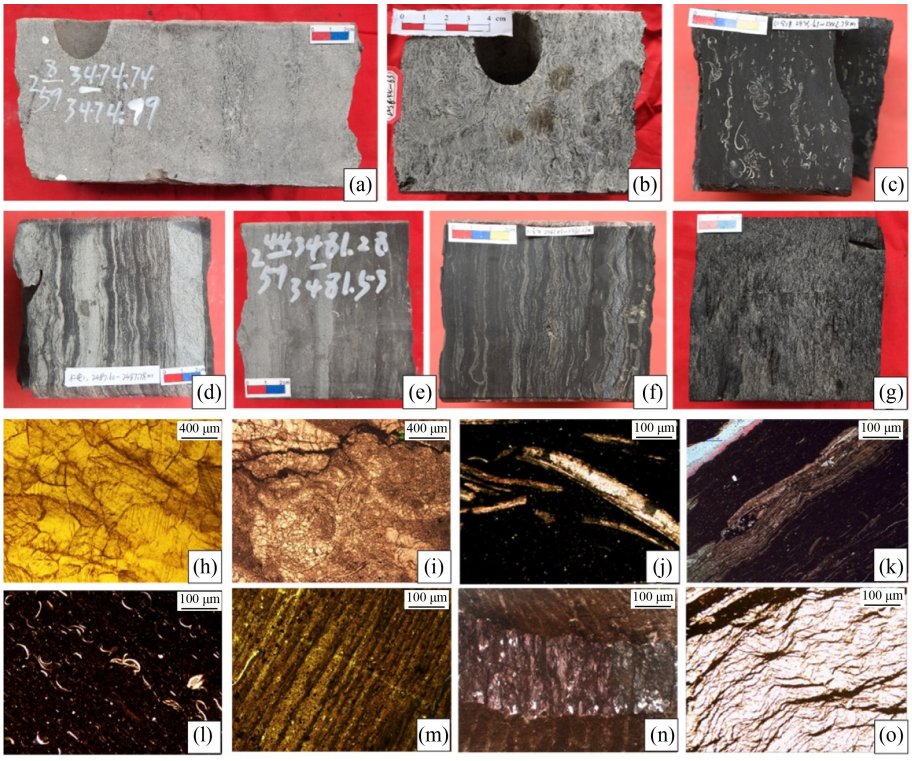

Fig. 8 Typical core photos and microscopic features of Da'anzhai Formation in Sichuan Basin. (a) Well RA1, 3474.74–7474.99 m, massive shell limestone; (b) well RA1, 2438.44–2438.63 m, massive argillaceous shell limestone; (c) well RA1, 2443.61–2443.74 m, massive shell-bearing shale; (d) well RA1, 2487.6–2487.78 m, centimeter-scale interbedding of shale and shell limestone (layered structure); (e) well RA1, 3481.28–3481.53 m, layered silty shale; (f) well RA1, 2436.95–2437.16 m, millimeter-scale interbedding of shale and shell limestone (laminated structure); (g) well RA1, 3292.99–3293.21 m, foliated pure shale; (h) well Q20, 2869.6 m, crystal calcites; (i) well Q25, 2859.18 m, micritic calcites; (j) well LA1, 3528.55 m, shell-bearing shale; (k) well G2, 2445.7 m, layered bioclastic and calcite veins; (l) well LA1, 3507.3 m, laminated shell-bearing shale; (m) well LA1, 2464.50 m, foliated mud and gray bands; (n) well NC2H, veined calcite in the hybrid sedimentary rocks; (o) well LA1, 3514.6 m, veined calcite with a superimposed structure.

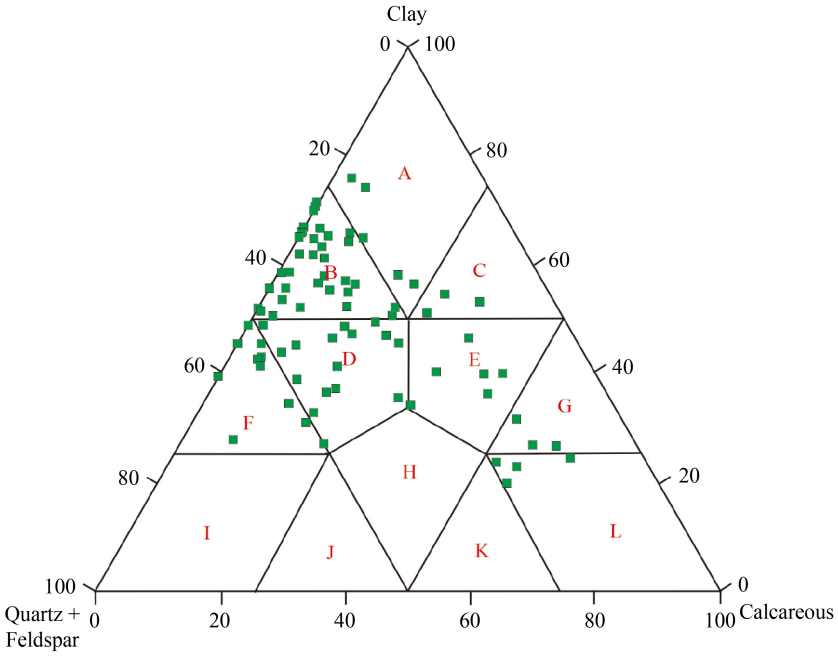

Fig. 9 Ternary diagram of shale mineral composition of Da'anzhai Formation in Sichuan Basin (A-clayey shale; B-silty-bearing clayey shale; C-shell-bearing clayey shale; D-silty shale; E- shell shale; F-argillaceous siltstone; G-argillaceous shell limestone; H-shell-bearing silty shale; I-siltstone; J- calcareous siltstone; K-silty limestone; L-shell limestone).

5.1.3 Lithological assemblages

Based on the vertical stacking characteristics of the lithofacies observed in the core wells and field outcrops (Fig. 11), lithofacies A was mainly distributed in D_1 and D_3 members. Lithofacies B is mainly distributed in the D_2a and D_2b sub-members. Lithofacies C and D are mainly developed in the D_2c sub-member. Lithofacies E and F occur mainly in the lower parts of the D_1 member and D_2a sub-member. Lithofacies G and H are predominantly present in the transition zone between the D_1 member and D_2a sub-member. Lithofacies I and J are mainly distributed in the D_2b sub-member.

Among these, lithofacies G and H represent delta plain facies restricted to the lake basin margin. They are often associated with lithofacies E and are < 3 m thick. Lithofacies E and F share similar structure characteristics, commonly co-occur, and are predominantly composed of by lithofacies F. Lithofacies D, which does not contain shells at all, rarely occurs and is associated with lithofacies C. Lithofacies A and B usually coexist. The Da'anzhai Formation comprises five main lithological assemblages: A, E–A, F–B, C–D, and I–J (Fig. 11).

5.2 Pore structure of main lithofacies

5.2.1 Microcosmic differences

The pore structure of shale influences its occurrence characteristics and fluidity of shale oil (Zargari et al., 2015; Zang et al., 2022). The pore structures of different rock samples from the Da'anzhai Formation were different. In the N_2 adsorption pore diameter distribution curve calculated by the Barrett-Joyner-Halenda (BJH) method, the H_2 type (Fig. 12(a)) was typically characterized by double peaks at 3–5 nm and 20–50 nm, indicating the coexistence of micropores and mesopores. The mixed type of H_2 and H_3 (Fig. 12(b)) was characterized by a single peak at 20–50 nm, indicating that mesopores were mainly developed. The H_3 type (Fig. 12(c)) and H_3 and H_4 mixed type (Fig. 12(d)) formed a single peak at 50–100 nm, indicating that macropores were mainly developed.

Corresponding to the mineral components, the specific surface area of the Da'anzhai Formation shale tended to increase with increasing clay content (Fig. 13(a)). At the same time, it decreased with increasing calcium content (Fig. 13(b)). This indicates that the recrystallization and dissolution of carbonate rocks in the Da'anzhai Formation were weak. Clay intergranular pores constituted the main reservoir space of shale oil.

The Da'anzhai Formation shale developed clay intergranular pores (Fig. 14(a)), pyrite intergranular pores (Fig. 14(i)), organic matter pores (Fig. 14(h)), quartz intergranular pores (Fig. 14(f)), calcite intergranular pores (Fig. 14(c)), organic matter edge pores (Figs. 14(g) and 14(h)), and microfractures (Figs. 14(d) and 14(e)). The morphology of the clay intergranular pores is complex (Fig. 14(a)). It is large-scale and distributed nearly linearly in the shale (Fig. 14(b)). Organic matter pores were mainly developed in amorphous asphaltenes (Fig. 14(h)) and were distributed in strips or irregular shapes. The organic matter pores in the target shale are poorly developed. Intergranular pores of calcite were formed

Code	Rock structure	Mineral composition/%				Lithofacies name	Core photo
		Siliceous	Calcareous	Clayey	Note		
A	Massive	< 25	> 50	< 25		Massive shell limestone	
B	Massive	< 25	> 50	25−50		Massive argillaceous shell limestone	
C	Massive	< 25	25−50	> 50		Massive shell-bearing clayey shale	
D	Massive	25−50	< 25	> 50		Massive clayey shale	
E	Layered	< 25	> 50	25−50		Layered argillaceous shell limestone	
F	Layered	< 25	25−50	25−50	Clayey >Calcareous	Layered shell shale	
G	Layered	25−50	< 25	25−50	Clayey >Siliceous	Layered silty shale	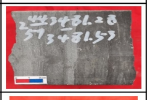
H	Layered	> 50	< 25	25−50		Layered argillaceous siltstone	
I	Laminated	< 25	< 25	> 50	Calcareous >Siliceous	Laminated shell-bearing shale	
J	Foliated	< 25	< 25	> 50	Siliceous >Calcareous	Foliated silty-bearing clayey shale	

Fig. 10 Lithofacies types of Da'anzhai Formation in the Sichuan Basin.

between the calcite crystals, with a regular shape, small aperture, and disconnection (Fig. 14(c)). It is almost undeveloped in the argillaceous and calcareous interbeds (Fig. 14(e)). These phenomena confirm that carbonate minerals make a very limited contribution to the reservoir properties.

5.2.2 Macroscopic differences

Because the N_2 adsorption experiment used powder samples, it can only reflect the micropores of rock and cannot characterize the influence of rock structure on reservoir properties. The HPMI experiment can obtain a wide range of pore diameters, which can be used to characterize the reservoir space characteristics of shale (Lu et al., 2018; Wang et al., 2019). The HPMI test results of the main lithofacies show that (Table 3, Fig. 6): lithofacies A and F had larger average Dp but smaller porosities,TPV, and SSA. In contrast, the average Dp of lithofacies J is smaller; however, its porosity, TPV, and SSA are larger. The Dp of lithofacies I and C is between those of the above two cases. This indicates that with an increase in shale content, the TPV of the lithofacies increases, but the Dp decreases. This is consistent with the N_2 adsorption experiments.

The T_2 values of NMR can be used to characterize the pore diameter distribution of shale from micrometers to nanometers, which is an effective full-aperture characterization method (An and Apostolos, 2002; Lu et al., 2018). By comparing the T_2 spectrum of NMR with the pore diameter distribution curve of HPMI based on the same sample and establishing the relationship between T_2 values and pore diameters, we can use the T_2 values to study the pore diameter distribution of rocks.

By jointly analyzing the NMR-T2 spectrum and HPMI pore diameter (r) distribution curve of the same lithofacies sample in the Da'anzhai Formation, and by establishing a conversion formula between T_2 value and pore diameter ($R = 10T_2$), the relative and absolute proportions of macropores, mesopores, and micropores in the different lithofacies were calculated (Fig. 15).

The contents of macropores in lithofacies A and F were relatively high, accounting for more than 75% on average. In contrast, the contents of micropores and mesopores were relatively low, accounting for less than 25% on average. The contents of micropores and mesopores in lithofacies C and I increased, accounting for more than 35%, and the content of macropores decreased

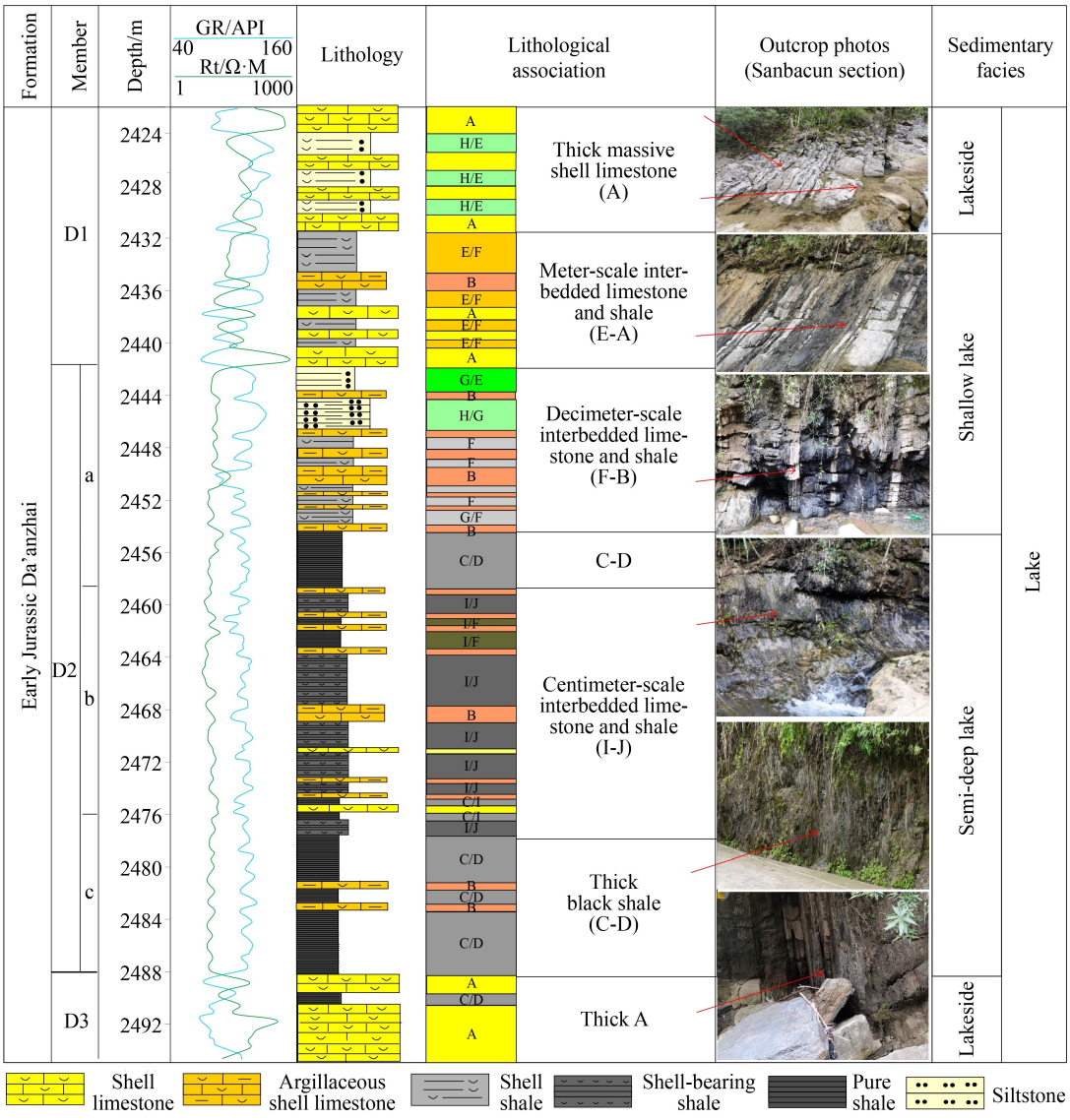

Fig. 11 Vertical variation characteristics of lithological assemblages (see Fig. 1 for the location of well RA1 and Sanbacun section).

accordingly. The contents of micropores and mesopores in lithofacies J were the highest, accounting for 80%, whereas the content of macropores was low, accounting for less than 20%. Comparing the proportion of pore diameters of various lithofacies, it was found that with an increase in shale content, the average pore diameter decreased (Fig. 15(a)), but the total pore volume increased. There were relatively more macropores in the layered, laminated, and foliated shales (Fig. 15(b)), related to the extremely developed bedding fractures in the rock structures.

5.3 Enrichment conditions and exploration direction of shale oil

5.3.1 Oil-bearing properties of different lithofacies

The oil saturation index (OSI = S_1/TOC, mg/g·TOC^{-1}) defined by Pepper (1991) can indicate the exploitable properties of shale oil. Jarvie (2012) suggested that shale oil reservoirs with OSI > 100 mg/g·TOC^{-1} exhibit good oil production pontential, while shale oil reservoirs with OSI less than 70 mg/g·TOC^{-1} are generally coonsidered non-recoverable. Wang et al. (2014) proposed that the shale oil reservoirs with OSI > 100 mg/g·TOC^{-1} exhibit the "Oil Crossover" phenomenon, which is a good, fractured shale oil reservoir.

The overall OSI values of the Da'anzhai Formation range from 10.6 to 339.2 mg/g·TOC^{-1}, with an average of 95.0 mg/g·TOC^{-1}. The OSI values of the lithofacies differed significantly (Fig. 16). The OSI values of lithofacies J are the largest, averaging 100.1 mg/g·TOC^{-1}, and 52.7% of samples with OSI > 100 mg/g·TOC^{-1}. The average OSI values are 98.2 mg/g·TOC^{-1} and 98.9 mg/g·TOC^{-1} for lithofacies I and F. The proportions of samples with OSI > 100 mg/g·TOC^{-1} are 40.0% and

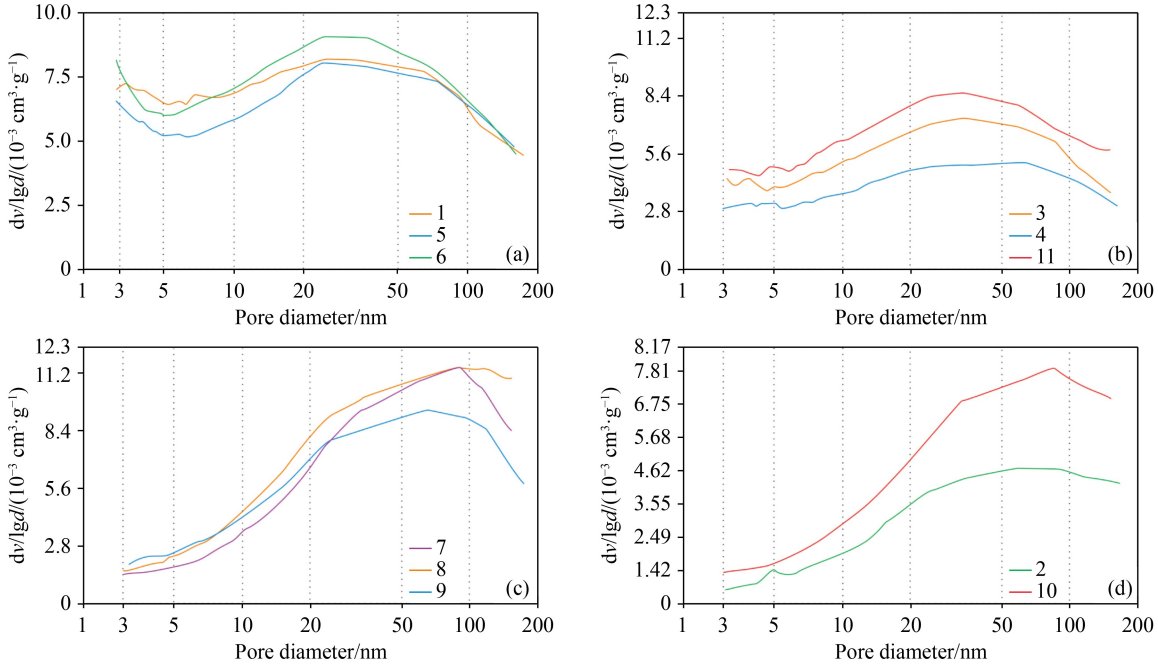

Fig. 12 Distribution of N_2 adsorption pore diameter of Da'anzhai Formation shale in Sichuan Basin. (a) H2 type; (b) mixed type of H2 and H3; (c) H3 type; (d) H3 and H4 mixed type. The sample information corresponding to the number is shown in .

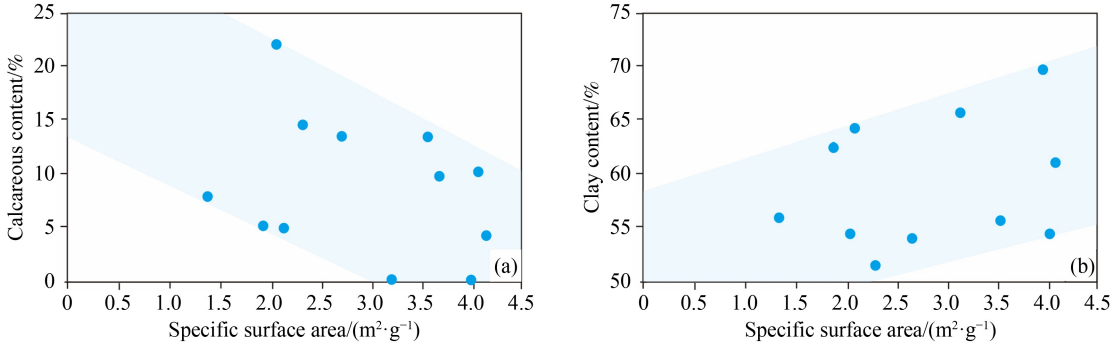

Fig. 13 Relationship between mineral composition and N_2 adsorption pore volume in Da'anzhai Formation, Sichuan Basin.

38.5%, respectively. The OSI values of lithofacies C were moderate, averaging 72.5 mg/g·TOC^{-1}. The samples with OSI > 100 mg/g·TOC^{-1} account for 26.7%. The OSI values of lithofacies A are small; the average value is only 49.8 mg/g·TOC^{-1}, and 20.0% of samples with OSI > 100 mg/g·TOC^{-1}.

The Da'anzhai Formation has unique characteristics compared with shale oil formations in North America and other basins in China. Shale oil in North America is produced primarily in marine formations. The primary shale oil production layers typically comprise fine sandstone, siltstone, and dolostone. They are characterized by high porosity and permeability. The clay mineral content in the shale oil production layers is generally less than 30% (He et al., 2023). The OSI in the sandstones or dolostones of the Williston Bakken Formation and Gulf of Mexico Eagle Ford Formation can reach up to 600 mg/(g·TOC^{-1}) (Jarvie, 2012), which determines that the interlayers are the most favorable targets for exploration.

The lithology of commercially developed shale oil reservoirs in China is similar to that of the reservoirs in North America. Fine sandstone, siltstone, and lacustrine carbonate interbeds are the main contributors to shale oil productivity in China. For example, the shale oil in the 7th member of the Triassic Yanchang Formation in the Ordos Basin is mainly produced from siltstone and fine sandstone interlayers (Guo et al., 2022). The shale oil production layer of the Lucaogou Formation in the Junggar Basin is dominated by silty dolomite and dolomitic siltstone (Zhi et al., 2023). The main exploration targets for shale oil in the Fengcheng Formation of the Mahu Depression are felsic shale or sandstone interlayers (Jiang et al., 2023).

In the Da'anzhai Formation, the degree of recrystallization of the shell limestone was relatively low, and the intercrystalline pores of calcite were undeveloped with small and independent pore sizes (Figs. 14(c), 14(d),

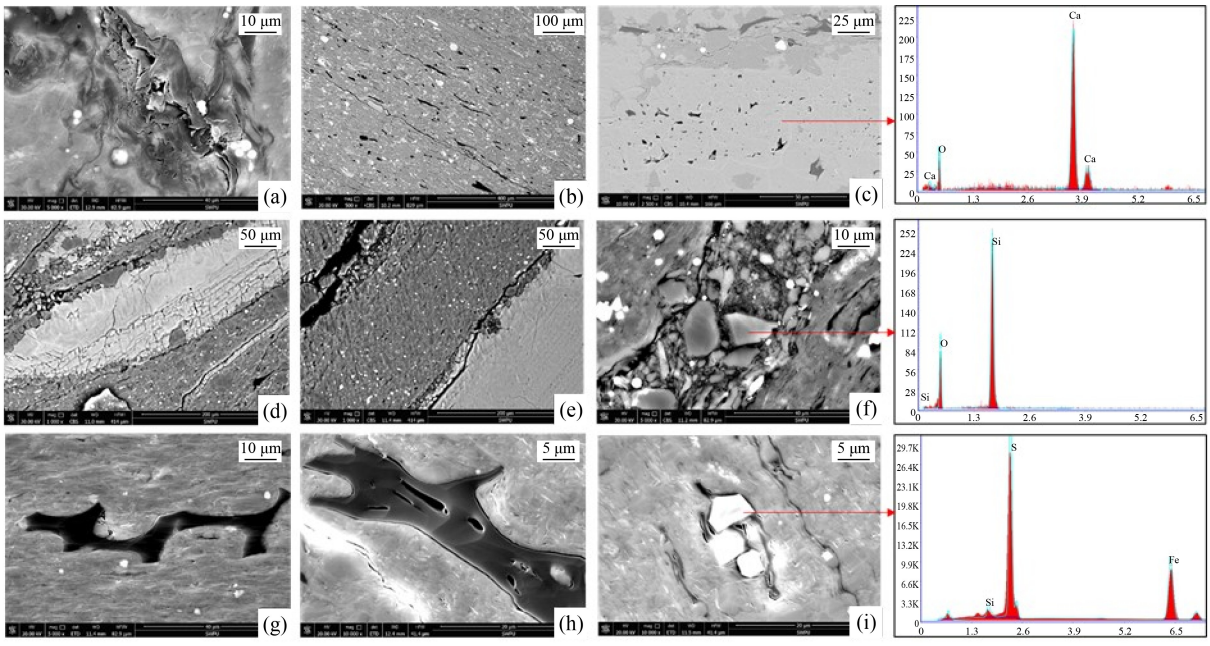

Fig. 14 Type of shale reservoir space of Da'anzhai Formation in Sichuan Basin. (a) well G6, 2535.18 m, clay mineral intragranular pores; (b) well G6, 2538.31 m, clay mineral intragranular pores distributed nearly linearly in shale; (c) well RA1, 2458.6 m, calcite intergranular pore; (d) well G6, 2538.31 m, calcite intergranular pores, and microcracks; (e) well G6, 2538.31 m, microfractures are developed between argillaceous and calcareous bands; (f) well G6, 2538.31 m, quartz intergranular pore; (g) well RA1, 2462.1 m, organic matter edge pore; (h) well RA1, 2464.5 m, organic matter pores; (i) well RA1, 2464.5 m, pyrite intergranular pore.

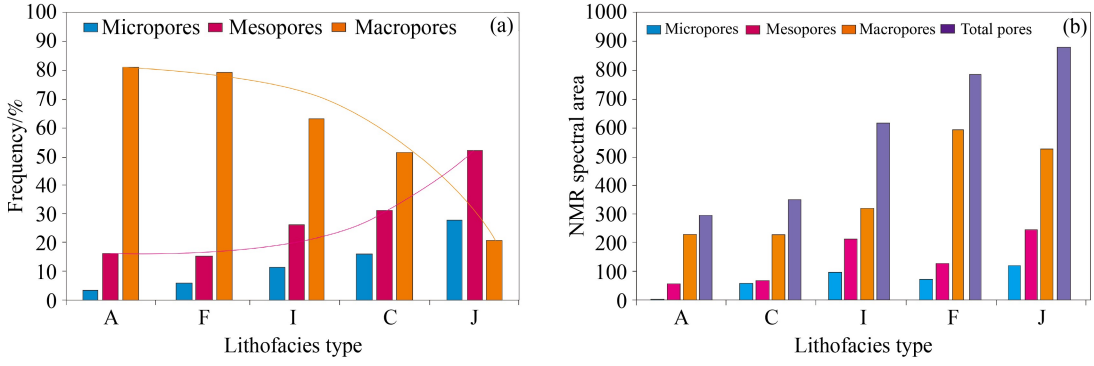

Fig. 15 Statistical histogram of the (a) relative percentage and (b) absolute proportion of pore diameter in different lithofacies of the Da'anzhai Formation.

and 14(e)). The physical properties of the shell limestone and hybrid sedimentary rocks were much worse than those of pure shale. The porosity and permeability of the reservoir increased with increasing shale content (Fig. 13). In the HPMI data (Table 2), the porosity of pure shale was five times that of shell limestone, and the mercury inflow is even 6.6 times that of shell limestone. The OSI value indicates that the oil content of the shell limestone and hybrid sedimentary rocks is lower than that of pure shale (Fig. 16), which is not conducive to shale oil enrichment. This also differs from the shale oil from the Shahejie Formation in the Bohai Bay Basin of China and the Barnett Formation in the Fort Worth Basin of North America. The organic-rich layered calcareous shale in these formations is a favorable target because the recrystallized intercrystalline pores in the calcite provide shale oil occurrence space (Jarvie et al., 2011; Li et al., 2022b, 2024; Liang et al., 2022). Therefore, shale oil exploration in sandstone or limestone interlayers is not feasible in the Da'anzhai Formation in the Sichuan Basin.

5.3.2 The importance of fracture systems for shale oil development

These results show that lithofacies I and J have the best reservoir properties and oil-bearing conditions in the Da'anzhai Formation. However, the clay content of pure shale is very high, and the pore diameter is small. Large adsorption and molecular forces exist between the fluid and the surrounding media in shale reservoirs, resulting in restricted oil flow (Zou et al., 2012; Ou and Li, 2017). To

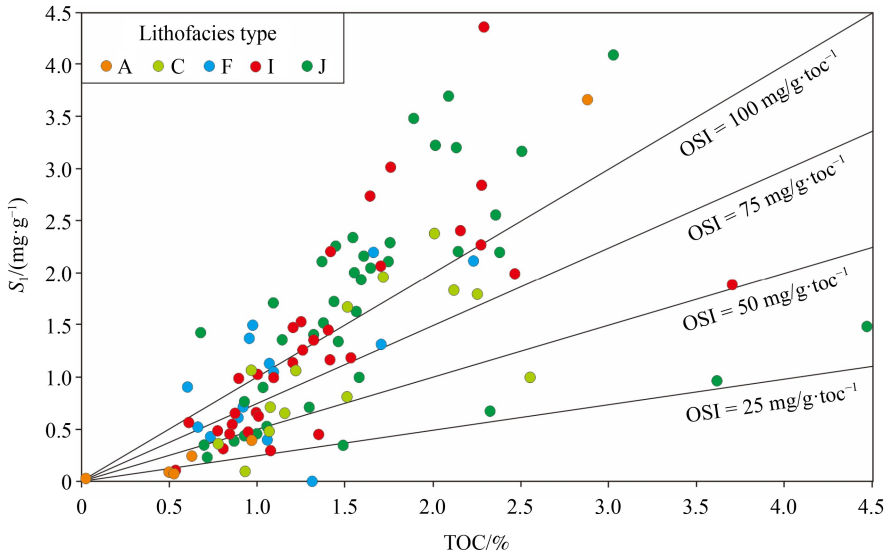

Fig. 16 Cross plot of S_1 and TOC of different lithofacies in Da'anzhai Formation.

achieve shale oil breakthroughs in such lithofacies, it is necessary to rely on the high oil content of the target reservoir (Xu et al., 2022). The average TOC value of the Da'anzhai Formation shale is only 1.38%, with an average S_1 value of 1.05 mg/g, indicating insufficient hydrocarbon richness to support the commercial development of pure shale-type shale oil.

Researchers generally agree that the development of bedding fractures enhances reservoir storage capacity, improves permeability, and plays a critical role in enhancing the effectiveness of subsequent hydraulic fracturing effect. These factors are essential for achieving high oil productivity in pure shale reservoirs (Jiang et al., 2020; Su et al., 2020; Liu et al., 2021a; Meng et al., 2021). Fractured shale oil does not require exceptionally high oil content for economic production. Therefore, fractured shale oil has a high commercial exploitation value in low-oil-bearing shale formations. The commercial breakthrough of pure shale oil from the Qingshankou Formation in the Gulong Sag and Shahejie Formation in the Jiyang Depression relies on both the high organic content and improved connectivity of pores and throats due to bedding fractures (Song et al., 2020; Pang et al., 2023).

The Da'anzhai Formation has mainly developed interlayer fractures, foliation fractures, and calcite joints. Interlayer fractures developed on the contact surface between the shale and limestone layers (Figs. 17(a), 17(c), and 17(d)). Foliation fractures are controlled by differential deposition rates and are formed on weak mechanical surfaces of shale (Meng et al., 2021). After being placed on the ground, a clear page-like structure was formed (Fig. 17(b)). Joint fissures mainly developed in the calcite veins. It is interconnected with the interlayer fractures and constitutes an effective seepage channel for shale oil (Figs. 17(c) and 17(d)). Many oil traces appeared in the carbonate interlayers of the layered shale in the core and field outcrops (Figs. 17(e) and 17(g)). The crude oil migrates along the joint and page fractures (Figs. 17(f) and 17(h)).

Therefore, for the Jurassic Da'anzhai Formation in the Sichuan Basin, shale oil has two enrichment modes. 1) Hybrid sedimentary rock-type shale oil. The key to the breakthrough of shale oil lies in finding vein calcite developed in interlayer fractures and joint fissures (Fig. 18(b)) rather than the simple interbedding of shell limestone and shale (Fig. 18(a)). 2) Pure shale-type shale oil. This shale oil must be commercially exploited with high oil content and highly developed foliation fractures (Fig. 18(c)). Massive shale was excluded because of undeveloped microcracks (Fig. 18(d)).

Various lithofacies of the Da'anzhai Formation were superimposed vertically. The dominant lithofacies were not concentrated in the fixed well section. In the comprehensive histogram of well RA1 (Fig. 11), the D_2b member (2458–2478 m) corresponds to the I-J lithological assemblage. The average TOC value of this section reaches 1.54%, the average S_1 value reaches 2.55 mg/g, the average OSI value reaches 160 mg/(g·toc^{-1}), and the average porosity value reaches 7.5%, indicating good oil content and reservoir property. Therefore, the D_2b member is a key exploration target for shale oil in the Da'anzhai Formation.

6 Conclusions

The Da'anzhai Formation can be divided into 10 lithofacies based on the rock structure and lithology. Massive shell limestone, massive shell-bearing clay shale, layered shell shale, laminated shell-bearing shale, and foliated silty-bearing clay shale are the five most typical

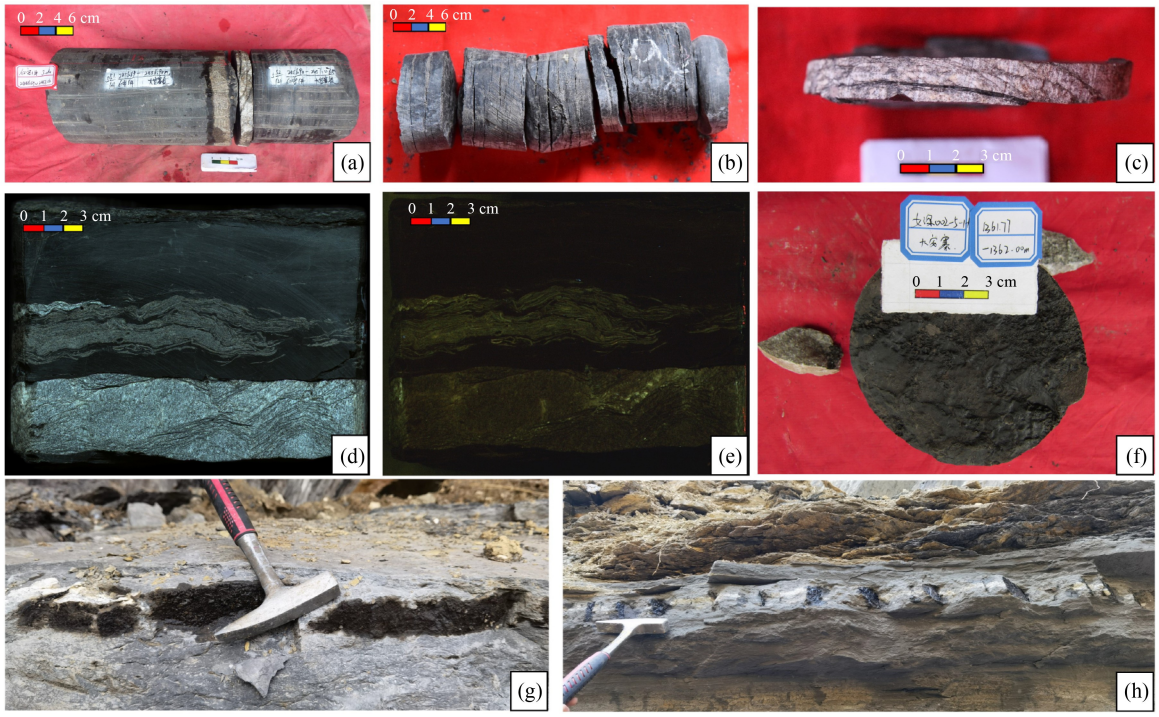

Fig. 17 Typical outcrops and core photos of the Jurassic Da'anzhai Formation in the Sichuan Basin. (a) Well RA1, 2456.69 m–2457.06 m, interlayer fractures; (b) well G10, 2473.14 m–2473.49 m, foliation fractures; (c) well RA1, 2462.78 m, calcite joints; (d) well RA1, 2459.46 m, joint fissures interconnecte with interlayer fractures; (e) well RA1, 2459.46 m, core fluorescence scanning; (f) well NS1, 1361.77 m, the foliation fracture is filled with oil; (g) Tieshan profile, oil seepage observed in centimeter scale limestone interlayer; (h) Tieshan profile, oil seepage observed from joint fissures).

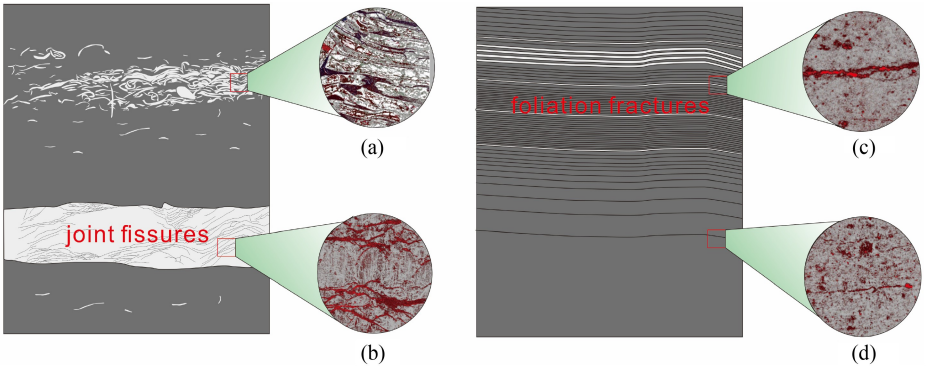

Fig. 18 Shale oil enrichment model of Jurassic Da'anzhai Formation in Sichuan Basin. (a) The oil content of bioclastic bands is poor; (b) shale oil is present in calcite joints and edge fractures; (c) shale oil is present in foliation fractures; (d) underdeveloped fractures in block shale with poor oil content.

lithofacies. Different lithofacies were superimposed in space and can be grouped into five main lithological assemblages.

The shale of the Da'anzhai Formation is dominated by clay intergranular pores, while dissolved pores are poorly developed. The pore diameter tended to decrease with an increase in clay content, but the total pore volume gradually increased. The physical properties of shale are significantly better than those of shell limestone. Bedding fractures constitute effective seepage channels for shale oil.

The Da'anzhai Formation has developed two types of shale oils. The breakthrough of hybrid sedimentary rock-type shale oil depends on vein calcite with interlayers and joint fractures. Pure shale-type shale oil must be commercially exploited with high oil content and highly developed foliation fractures. The I-J lithological assemblage of the D_2b sub-member is a favorable section for shale oil exploration.

Acknowledgments During the process of conducting this study, we received guidance from Professors Shijia Chen, Xingzhi Wang, Haihua Zhu, and Deming Zeng from Southwest Petroleum University. Senior engineers Benjian Zhang, Zhenglin Cao, and Haitao Hong from the Exploration and Development Research Institute of Southwest Oil and Gas

Field Company provided assistance within their capabilities. The author expresses loyal gratitude to the above-mentioned experts. This achievement is funded by the Science and Technology Cooperation Project of the CNPC-SWPU Innovation Alliance (No. 2020CX050000).

Competing interests The authors declare that they have no competing interests.

References

An M, Apostolos K (2002). An evaluation of the application of low field NMR in the characterization of carbonate reservoirs. SPE Annual Technical Conference and Exhibition. San Antonio, Texas: SPE, SPE-77401-MS

ARI (2015). World Shale Gas and Shale Oil Resource Assessment. Arlington: U.S. Energy Information Administration

Bai C Y, Yu B S, Han S J, Shen Z H (2020). Characterization of lithofacies in shale oil reservoirs of a lacustrine basin in eastern China: implications for oil accumulation. J Petrol Sci Eng, 195: 107907

Chen C, Yang X F, Wang X Z, Li B, Huang Z S, Tang R F, Du Y (2020). Sedimentary facies analysis of lacustrine carbonate in the Da'anzhai Formation, Ziliujing Formation, Lower Jurassic, in northeastern Sichuan Basin. Geological Review, 66(4): 836–852 (in Chinese)

Clarkson C R, Jensen J L, Blasingame T A (2011). Reservoir engineering for unconventional gas reservoirs: what do we have to consider? In: The Society of Petroleum Engineers North American Unconventional Gas Conference and Exhibition, Woodlands, Texas, June 12–16

EIA (2015). World shale resource assessments. Arlington: U.S. Energy Information Administration

Elika N Y, Elikb O Z, Altunsoyb M (2006). The interpretation of Rock-Eval data using graphs of S_2 vs. TOC: Middle Triassic-Lower Jurassic units, eastern part of SE Turkey. J Petrol Sci Eng, 53(1−2): 34–46

Feng C Y, Melnyk S, Ross C, Shanley K, Zonneveld J P, Gingras M K (2021). Lithofacies-dependent pore-throat radii and reservoir properties in the Lower Triassic Montney Formation, Puskwaskau Field, Alberta. Mar Pet Geol, 131: 105157

Guo Q L, Yao Y, Hou L H, Tang S H, Pan S Q, Yang F (2022). Oil migration, retention, and differential accumulation in "sandwiched" lacustrine shale oil systems from the Chang 7 member of the Upper Triassic Yanchang Formation, Ordos Basin, China. Int J Coal Geol, 261: 104077

Han H, Cao Y, Chen S J, . Lu J G, HuangC X, Zhu H H, Zhan P, Gao Y (2016). Influence of particle size on gas-adsorption experiments of shales: An example from a Longmaxi Shale sample from the Sichuan Basin, China. Fuel, 186: 750–757

He W Y, Bai X F, Meng Q A, Li J H, Zhang D Z, Wang Y Z (2022). Accumulation geological characteristics and major discoveries of lacustrine shale oil in Sichuan Basin. Acta Petrol Sin, 43(7): 885–898

He W, Zhu R, Cui B, Zhang S, Meng Q, Bai B, Feng Z, Lei Z, Wu S, He K, Liu H, Sun L (2023). The geoscience frontier of Gulong Shale Oil: revealing the role of continental shale from oil generation to production. Engineering, 28: 79–92

Hickey J J, Henk B (2007). Lithofacies summary of the Mississippian Barnett shale, Mitchell 2 T. P. Sims well, Wise County, Texas. AAPG Bull, 91(4): 437–443

Hu S Y, Bai B, Tao S Z, Bian C S, Zhang T S, Chen Y Y, Liang X W, Wang L, Zhu R K, Jia J H, Pan Z J, Li S Y, Liu Y X (2022). Heterogeneous geological conditions and differential enrichment of medium and high maturity continental shale oil in China. Pet Explor Dev, 49(2): 257–271

Jarvie D M (2012). Components and processes affecting producibility and commerciality of shale resource systems. Wuxi: Shale Oil Symposium

Jarvie D M, Coskey R J, Johnson M S (2011). The geology and geochemistry of the Parshall Area, Mountrail County, North Dakota. In: Robinson J W, LeFever J A, Gaswirth S B, eds. The Bakken-Three Forks Petroleum System in the Williston Basin. Rocky Mountain Association of Geologists Bakken Guidebook, Chapter 7, 229–281

Jiang C Z, Wang G W, Song L T, Huang L L, Wang S, Zhang Y L, Huang Y Y, Dai Q Q, Fan X Q (2023). Identification of fluid types and their implications for petroleum exploration in the shale oil reservoir: a case study of the Fengcheng Formation in the Mahu Sag, Junggar Basin, Northwest China. Mar Pet Geol, 147: 105996

Jiang Z X, Song Y, Tang X L, Li Z, Wang X M, Wang G Z, Xue Z X, Li X, Zhang K, Chang J Q, Qiu H Y (2020). Controlling factors of marine shale gas differential enrichment in southern China. Pet Explor Dev, 47(3): 661–673

Langford F F, Blanc-Valleron M M (1990). Interpreting Rock-Eval data using graphs of pyrolizable coals vs. total organic carbon. AAPG Bull, 74(6): 799–804

Lazar O R, Bohacs K M, Macquaker J H S, Schieber J, Demko T M (2015). Capturing key attributes of finegrained sedimentary rocks in outcrops, cores, and thin sections: nomenclature and description guidelines. J Sediment Res, 85(3): 230–246

Lei W Z, Chen D X, Liu Z Y, Cheng M (2023). Paleoenvironment-driven organic matter accumulation in lacustrine shale mixed with shell bioclasts: a case study from the Jurassic Da'anzhai member, Sichuan Basin (China). J Petrol Sci Eng, 220: 111178

Li M, Wang M, Zhang L B, Wang Q B, Wang X, Li X Q, Deng Z X, Dong S D (2024). Understanding pore space and oil content of liquid-rich shale in the southern Bohai Sea, China. Geoenergy Science and Engineering, 233: 212552

Li T W, Liu B, Zhou X N, Yu H, Xie X L, Xie Z H, Wang X Y, Rao H W (2022a). Classification and evaluation of shale oil enrichment: lower third member of Shahejie Formation, Zhanhua Sag, Eastern China. Mar Pet Geol, 143: 105824

Li Y, Chen S J, Wang Y X, Su K M, He Q B, Qiu W, Xiao Z L (2020). Relationships between hydrocarbon evolution and the geochemistry of solid bitumen in the Guanwushan Formation, NW Sichuan Basin. Mar Pet Geol, 111: 116–134

Li Y, Zhao Q M, Lyu Q, Xue Z J, Cao X P, Liu Z P (2022b). Evaluation technology and practice of continental shale oil development in China. Pet Explor Dev, 49(5): 1098–1109

Liang C, Wu J, Cao Y C, Liu K Y, Khan D (2022). Storage space

development and hydrocarbon occurrence model controlled by lithofacies in the Eocene Jiyang Sub-basin, East China: significance for shale oil reservoir formation. J Petrol Sci Eng, 215: 110631

Liu B, Shi J X, Fu X F, Lyu Y F, Sun X D, Gong L, Bai Y F (2018). Petrological characteristics and shale oil enrichment of lacustrine fine-grained sedimentary system: a case study of organic-rich shale in first member of Cretaceous Qingshankou Formation in Gulong Sag, Songliao Basin, NE China. Pet Explor Dev, 45(5): 884–894

Liu B, Sun J H, Zhang Y Q, He J L, Fu X F, Yang L, Xing J L, Zhao X Q (2021b). Reservoir space and enrichment model of shale oil in the first member of Cretaceous Qingshankou Formation in the Changling Sag, southern Songliao Basin, NE China. Pet Explor Dev, 48(3): 608–624

Liu D Q, Ge H K, Shen Y H, Liu H, Zhang Y (2021a). Experimental investigation on imbibition characteristics of shale with highly developed bedding fractures. J Nat Gas Sci Eng, 96: 104244

Liu Y, Qiu N, Yao Q, Chang J, Xie Z (2016). Distribution, origin and evolution of the Upper Triassic overpressures in the central portion of the Sichuan Basin, SW China. J Petrol Sci Eng, 146: 1116–1129

Liu Z B, Liu G X, Hu Z Q, Feng D J, Zhu T, Bian R K, Jiang T, Jin Z G (2020). Lithofacies types and assemblage features of continental shale strata and their implications for shale gas exploration: a case study of the Middle and Lower Jurassic strata in the Sichuan Basin. Nature Gas Industry B, 7(4): 358–369

Loucks R G, Ruppel S C (2007). Mississippian Barnett Shale: lithofacies and depositional setting of a deep-water shale-gas succession in the Fort Worth Basin, Texas. AAPG Bull, 91(4): 579–601

Lu S F, Li J Q, Zhang P F, Xue H T, Wang G L, Zhang J, Liu H M, Li Z (2018). Classification of microscopic pore-throats and the grading evaluation on shale oil reservoirs. Pet Explor Dev, 45(3): 452–460

Meng Q F, Hao F, Tian J Q (2021). Origins of non-tectonic fractures in shale. Earth Sci Rev, 222: 103825

Mohammed I Q, Farouk S, Mousa A, Lawa F A (2022). Lithofacies types, mineralogical assemblages and depositional model of the Maastrichtian–Danian successions in the Western Desert of Iraq and eastern Jordan. J Afr Earth Sci, 186: 104397

Nabawy B S, Lashin A A, Barakat M K (2022). Implementation of lithofacies and microfacies types on reservoir quality and heterogeneity of the Late Cretaceous Upper Bahariya Member in the Shurouk Field, Shoushan Basin, North Western Desert, Egypt. J Asian Earth Sci, 224: 105014

Ou C H, Li C C (2017). 3D discrete network modeling of shale bedding fractures based on lithofacies characterization. Pet Explor Dev, 44(2): 336–345

Pang X J, Wang G W, Kuang L C, Zhao F, Li C L, Wang C Y, Zhang M, Lai J (2023). Lamellation fractures in shale oil reservoirs: recognition, prediction and their influence on oil enrichment. Mar Pet Geol, 148: 106032

Pepper A S (1991). Estimating the petroleum expulsion behaviour of source rocks: a novel quantitative approach. Spec Publ Geol Soc Lond, 59(1): 9–31

Song M S, Liu H M, Wang Y, Liu Y L (2020). Enrichment rules and exploration practices of Paleogene shale oil in Jiyang Depression, Bohai Bay Basin, China. Pet Explor Dev, 47(2): 242–253

Su K M, Lu J G, Zhang G W, Chen S J, Li Y, Xiao Z L, Wang P, Qiu W (2018). Origin of natural gas in Jurassic Da'anzhai Member in the western part of central Sichuan Basin, China. J Petrol Sci Eng, 167: 890–899

Su K M, Lu J G, Zhang H X, Chen S J, Li Y, Xiao Z L, Qiu W, Han M M (2020). Quantitative study on hydrocarbon expulsion mechanism based on micro-fracture. Geoscience Frontiers, 11(6): 1901–1913

Wang M, Ma R, Li J B, Lu S F, Li C M, Guo Z Q, Li Z (2019). Occurrence mechanism of lacustrine shale oil in the Paleogene Shahejie Formation of Jiyang Depression, Bohai Bay Basin, China. Pet Explor Dev, 46(4): 833–846

Wang M, Shi L, Wang W, Huang A H, Chen G H, Tian S S (2014). Comparative study on geochemical characteristics of shale oil between China and U. S. A. Lithologic Reservoirs, 26(3): 67–74

Wang X, Wang M, Zhao C, Yang X Y, Jia Y D, Wu R, Li T Y, Zhao X B, Tang Y L (2024). Reservoir characteristics and controlling factors of the middle–high maturity multiple lithofacies reservoirs of the Lianggaoshan Formation shale strata in the northeastern Sichuan basin, China. Marine and Petroleum Geology, 161: 106692

Xiao Z L, Chen S J, Zhang S M, Zhang R, Zhu Z Y, Lu J G, Li Y, Yin X D, Tang L X, Liu Z H, Lin Z H (2021). Sedimentary environment and model for lacustrine organic matter enrichment: lacustrine shale of the Early Jurassic Da'anzhai Formation, central Sichuan Basin, China. J Palaeogeograph, 10(4): 584–601

Xu Q L, Liu B, Song X M, Wang Q P, Chen X D, Li Y, Zhang Y (2023). Hydrocarbon generation and organic matter enrichment of limestone in a lacustrine mixed sedimentary environment: a case study of the Jurassic Da'anzhai member in the central Sichuan Basin, SW China. Petrol Sci, 20(2): 670–688

Xu Y, Lun Z M, Pan Z J, Wang H T, Zhou X, Zhao C P, Zhang D F (2022). Occurrence space and state of shale oil: a review. J Petrol Sci Eng, 211: 110183

Yue H W, Vieth-Hillebrand A, Han Y J, Horsfield B, Schleicher A M, Poetz S (2021). Unravelling the impact of lithofacies on the composition of NSO compounds in residual and expelled fluids of the Barnett, Niobrara and Posidonia formations. Org Geochem, 155: 104225

Zang Q B, Liu C L, Awan R S, Yang X Y, Li G X, Wu Y P, Lu Z D, Feng D H (2022). Occurrence characteristics of the movable fluid in heterogeneous sandstone reservoir based on fractal analysis of NMR data: a case study of the Chang 7 Member of Ansai Block, Ordos Basin, China. J Petrol Sci Eng, 214: 110499

Zargari S, Canter K L, Prasad M (2015). Porosity evolution in oil-prone source rocks. Fuel, 153: 110–117

Zhang P F, Lu S F, Li J Q, Chang X C, Lin Z Z, Chen G, Li J J, Liu J Z, Tian S S (2022b). Evaluating microdistribution of adsorbed and free oil in a lacustrine shale using nuclear magnetic resonance: A theoretical and experimental study. J Petrol Sci Eng, 212: 110208

Zhang S M, Xiao Z L, Zhang R, Liu Z H, Li Y C, Tang L X, Bai R, Lin Z H (2022a). Geochemical characteristics and shale oil exploration potential of the Da'anzhai Formation in the Sichuan Basin, southwest China. Interpretation, 10(3): 469–482

Zhao W Z, Hu S Y, Hou L H, Yang T, Li X, Guo B C, Yang Z (2020). Types and resource potential of continental shale oil in China and its boundary with tight oil. Pet Explor Dev, 47(1): 1–11

Zhi D M, Xiang B L, Zhou N, Li E T, Zhang C J, Wang Y C, Cao J (2023). Contrasting shale oil accumulation in the upper and lower sweet spots of the lacustrine Permian Lucaogou Formation, Junggar Basin, China. Mar Pet Geol, 150: 106178

Zou C N, Yang Z, Cui J W, Zhu R K, Hou L H, Tao S Z, Yuan X J, Wu S T, Lin S H, Wang L, Bai B, Yao J L (2013). Formation mechanism, geological characteristics and development strategy of nonmarine shale oil in China. Pet Explor Dev, 40(1): 15–27

Zou C N, Yang Z, Tao S Z, Li W, Wu S T, Hou L H, Zhu R K, Yuan X J, Wang L, Gao X H, Jia J H, Guo Q L (2012). Nano-hydrocarbon and the accumulation in coexisting source and reservoir. Pet Explor Dev, 39(1): 15–27